Improving Spatial Resolution and Selectivity of Transcorneal Electrical Stimulation by Temporal Interference Technology

Author:
Ma, S; Song, X; Guo, T; Zhou, F; Liu, Z; Chai, X; Li, L

Publication details:
Proceedings of the Annual International Conference of the IEEE Engineering in Medicine and Biology Society, EMBS
v. 00
Medium: Print
pp. 1 - 4
9798350324471 (ISBN)
1557-170X (ISSN); 2694-0604 (ISSN)

Event details:
2023 45th Annual International Conference of the IEEE Engineering in Medicine & Biology Society (EMBC)
United States
2023-07-24 - 2023-07-27

Publication Date:
2023-01-01

Publisher DOI:
https://doi.org/10.1109/EMBC40787.2023.10341049

2023 45th Annual International Conference of the IEEE Engineering in Medicine & Biology Society (EMBC) | 979-8-3503-2447-1/23/$31.00 ©2023 IEEE | DOI: 10.1109/EMBC40787.2023.10341049

Improving Spatial Resolution and Selectivity of Transcorneal Electrical Stimulation by Temporal Interference Technology*

Saidong Ma, Xiaoyu Song, Tianruo Guo, *Senior Member, IEEE,* Feng Zhou, Zhengyang Liu, Xinyu Chai*, Member, IEEE,* Liming Li. *Member, IEEE*

***Abstract*— Transcorneal electrical stimulation (TES) used in a therapeutic device has been demonstrated significant neuroprotective effect for rescuing retinal function. However, the diffuse electric field induced by conventional TES devices reduced their spatial resolution and selectivity, limiting their capability of actively stimulating a severely diseased retina. A cutting-edge neuromodulation approach named temporal interference stimulation (TIS) was reported to induce electric fields focalizing on local neuronal targets. Despite the competent feasibility of application in retinal TIS, the interpretation of characteristics of spatial resolution and selectivity under TIS remains rudimentary. In this study, we conduct *in silico* investigations to understand the characteristics of spatial selectivity and resolution using a finite element model of a multi-layered eyeball and multiple electrode configuration. By simulating different metrics of electric potentials envelope modulated by TIS, our model supports the possibility of achieving mini-invasive and spatially selective electrical stimulation using retinal TIS. These simulations provide theoretical evidence on the basis of which sophisticated devices for improved spatial selectivity can be designed.**

***Clinical Relevance*— This study provides a theoretical basis for understanding how the design of electrode configuration impacts transcorneal TIS performance. This model can guide future development of transcorneal TIS configurations and stimulation strategies that may benefit patients with inherited retinal diseases.**

I. Introduction

Transcorneal electrical stimulation (TES) is capable of delaying retinal degenerative progress by providing neuroprotective effect of chronic stimulation with low-level electrical current [1], [2]. However, conventional TES settings cannot induce focused activation due to the diffuse electric field [3]-[5], limiting their utility in neuromodulation if we want to use TES to create prosthetic vision. Therefore, whether TES can be used as a retinal prosthetic device actively stimulating a severely degenerated retina, is still an open question.

Temporal interference stimulation (TIS) has been reported as a non-invasive neuromodulation technique enabling to selectively target local neurons in brain stimulation [6] and peripheral nerve stimulation [7]. This technique was achieved by interference of multiple electric fields induced by external electrodes. Each electrode delivers high-rate sinusoidal currents with a tiny difference. Interference between multiple electric fields created a prominent electric field envelope which can selectively stimulate the local neurons without co-active the overlying or off-target tissues. The amplitude of envelope induced by TIS depends on the superimposition of amplitudes in multiple channels and electrode distribution. The electric field geometry could be modulated by re-designing the electrode configuration and parameters.

More recently, the possibility of TIS technology in transcorneal neuromodulation was investigated by setting a finite element model of eyeball and transcorneal stimulation electrodes [8]. This study discussed the feasibility of retinal TIS from the perspective of distributions of electric fields, but the optimal electrode parameter spaces of TIS for improved focality are not yet explored. In another modeling study, the direct influence of retinal ganglion cell (RGC) morphological and biophysical properties on TIS efficacy was simulated [9]. However, this preliminary study only simulated the stimulus-RGC response with fixed TIS settings, without considering the impact of different electrode properties.

In this study, we hypothesized that spatial resolution and selectivity could be quantitatively controlled by re-designing the electrode configuration and stimulation parameters, so maximize the perceptual efficacy of prosthetic vision. We began by building an anatomically-accurate human eyeball model with multi-transcorneal electrodes, capable of exploring how different electrode settings influence the performance of transcorneal TIS *in silico*. We then assessed how electrode size and locations affect the envelope of electric potentials in the posterior eyeball. Our model provides an effective tool to design next-generation transcorneal devices and therapeutic stimulation strategies toward more focused TES.

II. Methods

A. A Finite Element Model of Eyeball and Transcorneal Electrical Stimulation

In Fig. 1A, a three-dimensional electrical model of eyeball and extraocular electrodes was constructed in the AC/ DC module of COMSOL Multiphysics 5.6 (COMSOL, Inc. Palo Alto, CA, USA). Multiple conductive layers were built to simulate basic structures of a human eyeball comprising sclera, choroid, retina, vitreous body, lens, atria, and cornea. To avoid edge effects, the entity of eyeball was wrapped in a filled cubical solution domain, whose conductivity was set the same as that of vitreous body. Platinum disc electrodes with a diameter of 1 mm and thickness of 50 μm were simulated. Under TIS conditions, the lower surfaces of electrodes were

*This research is supported by The National Natural Science Foundation of China (61671300, 61971280, 62073221).

S. Ma, X. Song, F. Zhou, Z. Liu, X. Chai and L. Li are with School of Biomedical Engineering, Shanghai Jiao Tong University, Shanghai, China.

T. Guo is with the Graduate School of Biomedical Engineering and Tyree Institute of Health Engineering, UNSW Sydney, NSW 2052, Australia.

E-mail for correspondence: lilm@sjtu.edu.cn

placed near the upper surface of the sclera (Fig. 1A). The properties of conductivity and thickness were modeled based on Su et al [8] and Lu et al [10].

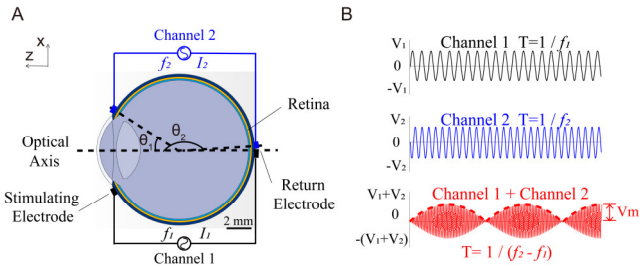

Figure 1. A finite element model of anatomically-detailed eyeball and transcorneal electrical stimulation. A: A cross section of the model of an eyeball with two stimulating channels (pairs). Each channel includes a stimulating electrode on sclera and a return electrode behand the eyeball. B: Stimulation waveform (blue and black lines: electric potential waveforms generated by channel 1 and 2; red dashed line: maximum value of electric potential envelope generated by superimposition of two channels)

B. Electrode Configuration and TIS parameters

As shown in Fig. 1B, two stimulating channels were set on the defined cross section plane. The line through the center of eyeball and the most convex point of the cornea was defined as the optical axis. Two channels were set to be axial symmetrical. In each channel, the electrode placed abutted the cornea was defined as stimulating electrode (θ_1), and the electrode placed near retina as return electrode (θ_2). θ_1/ θ_2 referred to the angles between stimulating electrodes / return electrodes and the optical axis, respectively. The frequency of channel 1 was denoted as f_1, and the frequency of channel 2 as f_2, while the frequency difference between channels was Δf ($f_2 = f_1 + \Delta f$). Channel 1 delivered an alternating sinusoidal current I_1, while channel 2 with a current I_2. The default phase difference between two channels was π.

To assess the TIS efficacy, the extracellular electric potential (EP) and the maximum value of the EP envelope (EP peak，V_m) under different TIS conditions were calculated. The value of the envelope at a given location was calculated by the superimposition of corresponding EP values generated by two channels (Fig. 1B). The superimposed waveform was modulated with the oscillating frequency of Δf. In this study, the EP peak value at a specific point under TIS was calculated based on (1):

$$V_m = V_1 + V_2 \tag{1}$$

where V_1 and V_2 represented the EP generated by two stimulating channels at the specific locations simultaneously.

The approach of current steering was implemented by changing the input currents between stimulating channels. To create additional stimulation local sites without affecting fixed electrode placement, the feasibility of current steering under TIS was evaluated with the ratio of current intensity delivered to the stimulating channels. I_1 and I_2 referred to the current intensity delivered by channels 1 and 2. The current ratio α was defined by:

$$\alpha = \frac{I_1}{I_1+I_2} \tag{2}$$

C. Analysis of maximum value of EP envelope

The patterns of spatial distribution of envelope over the retina were classified into two types, 1) a unimodal pattern manifesting a single peak near central retina, 2) a non-unimodal pattern.

To evaluate the characteristics of spatial resolution and selectivity, metrics of maximum value of envelope EP over the retina were stimulated: 1) peak value: defined as the maximum value of unimodal EP waveform, 2) peak offset: defined as the maximum angle between the positions of unimodal peaks when current ratios changed. and 3) peak width, defined as the distance between both sides of a unimodal peak measured at 90% of the peak height These metrics reflected modulated ranges of envelop EP distributions which could be used as indicators of spatial resolution and selectivity by TIS.

III. RESULTS

A. Analysis of Spatial Distribution of Maximum Value of EP Envelope Under TIS

The influence of different electrode parameters on spatial distribution of EP peak was evaluated under TIS. Different parameters containing 8 electrode sizes (radius from 0.25 mm to 2 mm), stimulating and return electrode positions (θ_1 from 5° to 35°, θ_2 from 171° to 177°), and current ratio α ranging from 0.1 to 0.5, were calculated under TIS.

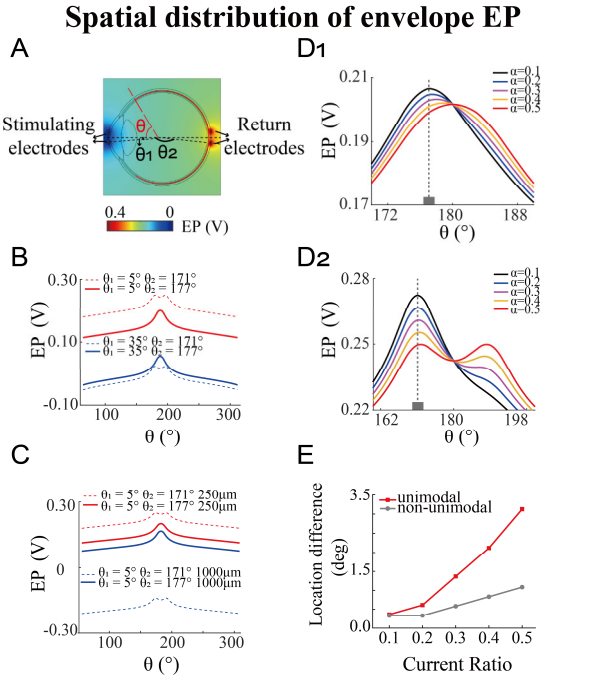

Figure 2. The influence of different electrode parameters on spatial distribution of EP peak. A: The spatial distribution of EP peak over the eyeball induced by different stimulating electrode (θ_1) and return electrode (θ_2) placements. B: The spatial distribution of EP peak over the retina induced by different stimulating and return electrode locations (θ_1 = 5°, 35°; θ_2 = 171°, 177°). C: The spatial distribution of EP peak over the retina induced by different electrode sizes (radius = 250 μm, 500 μm, 750 μm, 1000 μm, and 1250 μm). D1: The spatial distribution of EP peak over the retina (unimodal pattern) induced by a range of intensity ratio (α = 0.1, 0.2, 0.3, 0.4, 0.5) with θ_1 = 5°, θ2 = 177°. D2: The spatial distribution of EP peak over the retina (non-unimodal pattern) induced by different intensity ratio with θ_1 = 5°, θ2 = 171°. (gray squares and dashed lines: locations of return electrode). E: The location differences in degree between the return electrodes and the peak locations of EP envelope in D1 and D2

To assess the effects of different electrode and stimulation parameters under TIS, the spatial distributions of EP peak over the observation domain of eyeball and retina were initially explored. The spatial distributions of maximum value of envelope EP were simulated over the observation domain of eyeball under TIS with the current amplitude set to 1mA. Fig. 2A indicates that when return electrodes are closer to posterior position of eyeball and stimulating electrodes near certain position of anterior eyeball ($\theta_1 = 5°$, $\theta_2 = 173°$, $175°$, $177°$), the EP peak reaches highest value near the return electrodes while lowest value near the stimulating electrodes. To further assess this phenomenon, corresponding spatial distributions of the EP peak over retina (defined as the red curve in the top left panel of Fig. 2A) was extracted with $\theta_1 = 5°$ and $35°$, while $\theta_2 = 171°$ and $177°$. Fig. 2B shows that the spatial distribution patterns vary with the change of θ_2 when fixing θ_1, while remain the same ones with the change of θ_1 when fixing θ_2. Moreover, Fig. 2C that distribution patterns are not changed by different of electrode sizes (both stimulating and return electrodes from radius of 250 μm to 1000 μm). To assess the effects of current steering, the spatial distributions of EP peak under different current ratios of unimodal patterns (Fig. 2D1) and of non-unimodal patterns (Fig. 2D2) were plotted respectively. Our results suggest the current ratios between electrodes tends to shift EP peak locations from where near one electrode (denoted as gray squares) towards another one. However, the two distribution patterns appear to differ the effects of shift. As illustrated in Fig. 2E, the corresponding peak values of unimodal pattern under different current ratios tend to grow more rapidly than that of non-unimodal pattern. These findings indicate that the unimodal patterns rather than non-unimodal ones reflect a better performance of spatial resolution and selectivity, which were to be validated by subsequent results.

B. *Influences of Current Ratios on EP Envelope Properties under TIS*

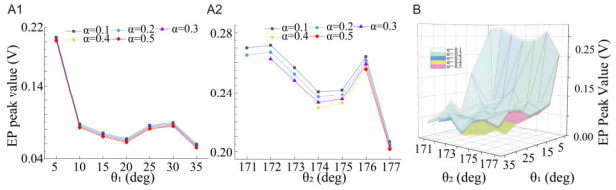

Figure 3. The influences of different current ratios on the peak values. A1: The influences of stimulating electrode positions on peak values under different current ratios. A2: The influences of return electrode positions on peak values under different current ratios. B: A perspective direction of electrode-dependent peak value under different current ratios.

The current ratio was used to evaluate the feasibility of steering approach with the metrics of aforementioned peak values to measure the spatial selectivity of TIS under fixed electrode placement. electrodes size was fixed at 1000 μm, and the peak values of envelope EP were calculated on the aforementioned range of electrode positions when current ratio changed from 0.1 to 0.5 with a step of 0.1. Fig. 3A1 shows the influence of stimulating electrode positions on peak values under different current ratios. When positions of return electrodes are fixed, the peak values decrease nonlinearly with the change of stimulating electrode positions. Additionally, the change of current ratios might not affect the peak values because curves with different colors are consistent with the patterns with slight differences among them. Fig. 3A2 shows the influence of return electrodes locations on peak values under different current ratios when fixing positions of stimulating electrodes. The peak values indicate a fluctuating trend with a sharp decline from 176° to 177°, but this range exhibits a steady tendency that the patterns can maintain unimodal when current ratios change. As shown in Fig. 3B, wholescale color fill surfaces of peak values of unimodal distribution patterns under different current ratios are plotted. It can be observed that the distribution of EP peak over the defined domain of electrode positions is nearly identical under different current ratios. However, the range of unimodal pattern decreases when current ratios are altered from 0.1 to 0.5. Moreover, both stimulating and return electrode positions have nonlinear influences on the distributions of peak values. Concerning the expected controllability of current ratios should not sacrifice available ranges of electrode positions when prioritizing the metric of peak values, our model suggests that the optimal electrode positions as θ_2 ranging from 176° to 177° and θ_1 ranging from 5° to 10°.

C. *Influences of current ratios on peak offsets of maximum value of EP envelope under TIS*

To further explore the effect of current ratio, the distributions of EP peak offset were calculated across the defined domain of different electrode positions. The values of EP peak offset were plotted as scatter. Nonlinear surface fitting was used to analyze the EP peak offset distributions, and further assess the spatial TIS-induced selectivity.

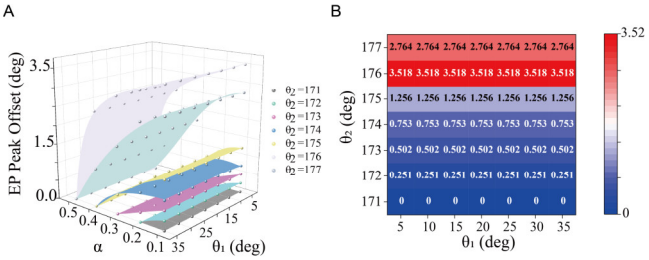

Figure 4. The influences of different current ratios on the peak offsets. A: Spatial distributions of the EP peak offset induced by different current ratios and electrode positions. B: Parameter space of the maximum EP peak offset over the defined domain of electrode positions.

The influences of different current ratios and electrode positions on the EP peak offsets were fitted into surfaces with a function named Rational Taylor. The current ratio, stimulating electrode position, and the return electrode position served as three variables during the surface fitting. In Fig. 4A, the shapes of fitted surfaces indicates different effects of the parameters on the EP peak offset. Variable of θ_1 cannot affect the value of peak offset, while variables of current ratio and θ_2 have a non-linear effects on the metrics. Fitted surfaces of $\theta_2 = 176°$ and $177°$ under different current ratios exceed above the others, which concurs with the relatively higher value of the peak offset at $\theta_2 = 176°$ and $177°$ (Fig. 4B). Based on these findings, optimal electrode positions of θ_2 ranging from 176° to 177° were preferred for practical stimulation.

D. *Influences of electrode sizes on peak width of maximum value of EP envelope under TIS*

The stimulation efficacy of non-invasive neuromodulation approaches could depend profoundly on the electrode

configurations and geometries. In this section, different electrode sizes (both stimulating and return electrodes) were modeled ranging from 250 µm to 2000 µm with a step of 250 µm.

In Fig. 5, the 90% peak widths of unimodal patterns vary with different electrode sizes. Smaller electrode sizes (< 1500 µm) induced lower values of peak widths (i.e., better focality). However, the range of electrode positions for unimodal presentation might be narrowed with smaller electrode sizes (< 750 µm). Larger electrode sizes (> 1250 µm) might account for incompatible implantation (gray position shown). By taking multiple factors (electrode positions range, surgical difficulty and resulted focality) into account together, our model suggested that electrodes ranging from 750 to 1250 µm should be more practical to use.

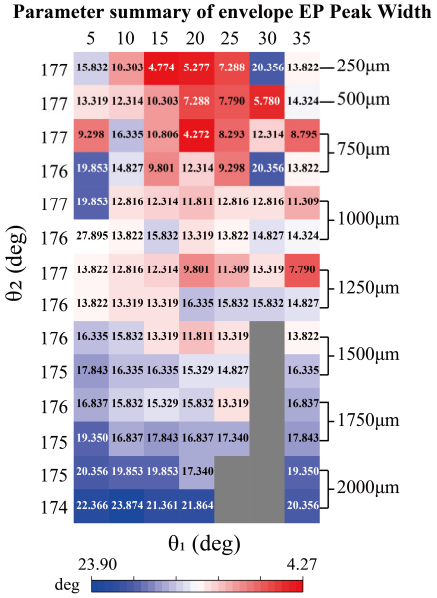

Figure 5. Parameter space summary of the maximum EP peak width over the defined domain of electrode positions.

IV. Discussion and Conclusion

In this study, influences of electrode and stimulation parameters on EP envelop properties were investigated under TIS. Our results showed that spatial distributions of EP envelope varied with unimodal and non-unimodal patterns, depending on the given parameters. In our model, the EF envelope distributions turned into single spike patterns when the return electrode was located near retinal side [8]. Grossman et al. [6] and Esmaeilpour et al. [11] used the envelope EF as markers to explain the mechanism underlying TIS-induced local activation. Gomez-Tames et al. [12] suggested the importance of EP/EF envelope parameters in indicating response of cortex neurons. However, the key parameters dominating the TIS-induced perceptual efficacy are still unclear. More investigations of neuronal activity under TIS. are needed. In addition, our model provided insights about how electrode parameters and current ratios impact the feasibility of current steering under TIS. Our results strongly supported the benefits of current steering in the characterizing TIS-induced focality and spatial selectivity, namely steering could be dominated by electrode distribution while minimally influenced by electrode sizes [6].

This model provides a platform of designing sophisticated device for transcorneal electrical stimulation used for creating artificial vision. Future studies will focus on improving the biological features of this model by adding retinal anatomical microstructures, active neuronal components, cell distribution towards more clinically relevant simulations. Other approaches for improving the spatial resolution by TIS, such as electrode distribution and geometries could be further tested.

References

[1] M. T. Pardue and R. S. Allen, "Neuroprotective strategies for retinal disease," *Progress in Retinal and Eye Research*, vol. 65, pp. 50–76, Jul. 2018.

[2] L. Yue, J. D. Weiland, B. Roska, and M. S. Humayun, "Retinal stimulation strategies to restore vision: Fundamentals and systems," *Progress in Retinal and Eye Research*, vol. 53, pp. 21–47, Jul. 2016.

[3] T. Morimoto, T. Fujikado, J.-S. Choi, H. Kanda, T. Miyoshi, Y. Fukuda, and Y. Tano, "Transcorneal electrical stimulation promotes the survival of photoreceptors and preserves retinal function in royal college of surgeons rats," *Investigative Ophthalmology & Visual Science*, vol. 48, no. 10, pp. 4725–4732, Oct. 2007.

[4] A. Schatz, T. Röck, L. Naycheva, G. Willmann, B. Wilhelm, T. Peters, K. U. Bartz-Schmidt, E. Zrenner, A. Messias, and F. Gekeler, "Transcorneal Electrical Stimulation for Patients with Retinitis Pigmentosa: A Prospective, Randomized, Sham-Controlled Exploratory Study," *Investigative Opthalmology & Visual Science*, vol. 52, no. 7, p. 4485, Jun. 2011.

[5] A. Schatz, J. Pach, M. Gosheva, L. Naycheva, G. Willmann, B. Wilhelm, T. Peters, K. U. Bartz-Schmidt, E. Zrenner, A. Messias, and F. Gekeler, "Transcorneal Electrical Stimulation for Patients With Retinitis Pigmentosa: A Prospective, Randomized, Sham-Controlled Follow-up Study Over 1 Year," *Investigative Opthalmology & Visual Science*, vol. 58, no. 1, p. 257, Jan. 2017.

[6] N. Grossman, D. Bono, N. Dedic, S. B. Kodandaramaiah, A. Rudenko, H.-J. Suk, A. M. Cassara, E. Neufeld, N. Kuster, L.-H. Tsai, A. Pascual-Leone, and E. S. Boyden, "Noninvasive Deep Brain Stimulation via Temporally Interfering Electric Fields," *Cell*, vol. 169, no. 6, pp. 1029-1041.e16, Jun. 2017.

[7] B. Botzanowski, M. J. Donahue, M. S. Ejneby, A. L. Gallina, I. Ngom, F. Missey, E. Acerbo, D. Byun, R. Carron, A. M. Cassarà, E. Neufeld, V. Jirsa, P. S. Olofsson, E. D. Głowacki, and A. Williamson, "Noninvasive Stimulation of Peripheral Nerves using Temporally-Interfering Electrical Fields," *Advanced Healthcare Materials*, vol. 11, no. 17, p. 2200075, Sep. 2022.

[8] X. Su, J. Guo, M. Zhou, J. Chen, L. Li, Y. Chen, X. Sui, H. Li, and X. Chai, "Computational Modeling of Spatially Selective Retinal Stimulation With Temporally Interfering Electric Fields," *IEEE Transactions on Neural Systems and Rehabilitation Engineering*, vol. 29, pp. 418–428, 2021.

[9] F. Zhou, X. Song, Z. Liu, X. Chai, and L. Li, "Influence of Morphological and Electrophysiological Parameters on Retinal Ganglion Cells Threshold under Temporal Interference Stimulation," presented at the 2021 14th International Congress on Image and Signal Processing, BioMedical Engineering and Informatics (CISP-BMEI), Shanghai, China.

[10] Z. Lu, M. Zhou, T. Guo, J. Liang, W. Wu, Q. Gao, L. Li, H. Li, and X. Chai, "An in-silicoanalysis of retinal electric field distribution induced by different electrode design of trans-corneal electrical stimulation," *Journal of Neural Engineering*, vol. 19, no. 5, Sep. 2022.

[11] Z. Esmaeilpour, G. Kronberg, D. Reato, L. C. Parra, and M. Bikson, "Temporal interference stimulation targets deep brain regions by modulating neural oscillations," *Brain Stimulation*, vol. 14, no. 1, pp. 55–65, Jan. 2021.

[12] J. Gomez-Tames, A. Asai, and A. Hirata, "Multiscale Computational Model Reveals Nerve Response in a Mouse Model for Temporal Interference Brain Stimulation," *Frontiers in Neuroscience*, vol. 15, p. 684465, Jun. 2021